Scaling Behaviors of LLM Reinforcement Learning Post-Training: An Empirical Study in Mathematical Reasoning

Anonymous ACL submission

Abstract

While scaling laws for large language models (LLMs) during pre-training have been extensively studied, their behavior under reinforcement learning (RL) post-training remains largely unexplored. This paper investigates the scaling behavior of Large Language Model (LLM) reinforcement learning post-training, focusing on mathematical reasoning. Through experiments across the Qwen2.5 series (0.5B to 72B), we characterize how model scale, data, and compute interact. Our analysis yields four key findings: ❶ Larger models consistently demonstrate superior compute and data efficiency. ❷ The relationship between model performance and training resources follows a **predictive power-law** across both base and instruction-tuned models. ❸ RL learning efficiency exhibits a latent **saturation trend** with increasing model scale. ❹ In data-constrained regimes, performance is primarily driven by the **total volume of training data** rather than sample uniqueness. These results offer practical guidelines for scaling reasoning capabilities through reinforcement learning post-training.

1 Introduction

The rapid progress of large language models (LLMs) has made elucidating their scaling laws a matter of central importance. These laws, which capture the intricate relationships between model architecture, parameter size, computational cost, data availability, and downstream performance (Kaplan et al., 2020; Hoffmann et al., 2022), are invaluable not only because they illuminate the latent factors governing learning dynamics, but also because they provide actionable guidance on how to distribute scarce computational resources most effectively (Li et al., 2025a). While extensive efforts have clarified scaling behavior, the scaling behavior of reinforcement learning (RL) post-training for LLM reasoning remains underexplored.

During pretraining, Kaplan et al. (2020) show that cross-entropy loss follows smooth power-law scaling in model size, dataset size, and training compute, implying that larger models trained for fewer steps are compute-optimal. Hoffmann et al. (2022) refine this by showing that, under fixed compute, scaling parameters and tokens proportionally is optimal, since many large models are undertrained. Extending to neural-based RL, Hilton et al. (2023) empirically demonstrates that the intrinsic performance of convolutional neural networks (CNNs) optimized via reinforcement learning also scales like power-law with model capacity and environment interaction.

While these works have established foundational scaling principles for pretraining and RL in smaller neural networks, RL has become the dominant post-training strategy for enhancing LLMs' reasoning abilities—especially in mathematics, a domain requiring long-horizon, compositional reasoning (Ferrag et al., 2025; DeepSeek-AI, 2025; Kimi Team, 2025; Ahn et al., 2024). However, despite its growing adoption for LLM reasoning tasks, a systematic understanding of how to effectively scale RL training remains elusive. In this work, we conduct a comprehensive empirical study to characterize these scaling behaviors across three critical resource regimes: (1) the **compute-constrained** scenario, where we determine the optimal model size to minimize test loss ($1 - PassRate$) under a fixed FLOPs budget; (2) the **data-constrained** scenario, where we identify the model size yielding the lowest test loss with limited unique samples; and (3) the **data reuse** scenario, where we explore the trade-off between data uniqueness and reuse intensity under a fixed total data volume.

Based on our analysis across these regimes, we propose a **predictive formulation** that characterizes the relationship between test loss L, model size N, and resource budget X (where X denotes either Compute C or Data D). We find that the

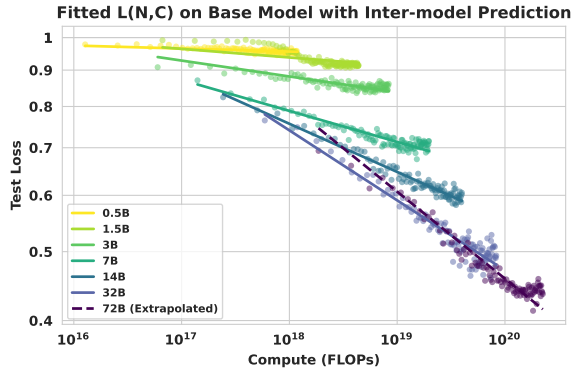

(a) Inter-model Prediction for Base Model

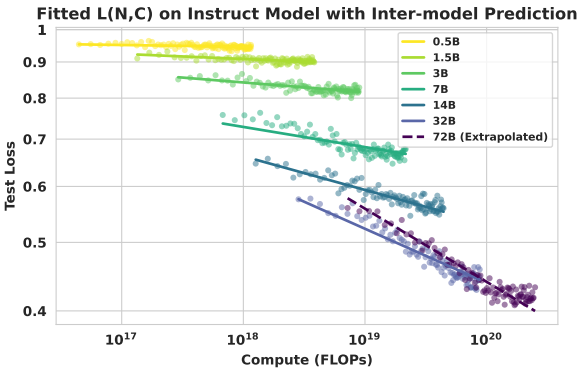

(b) Inter-model Prediction for Instruct Model

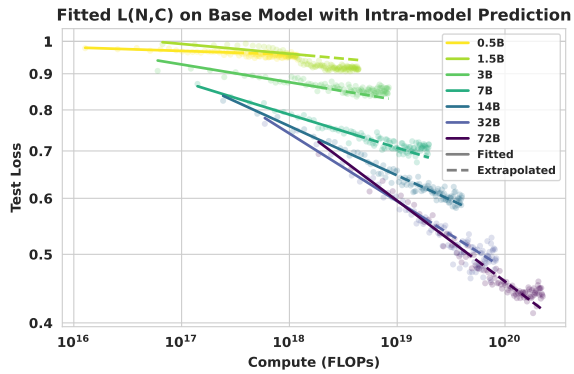

(c) Intra-model Prediction for Base Model

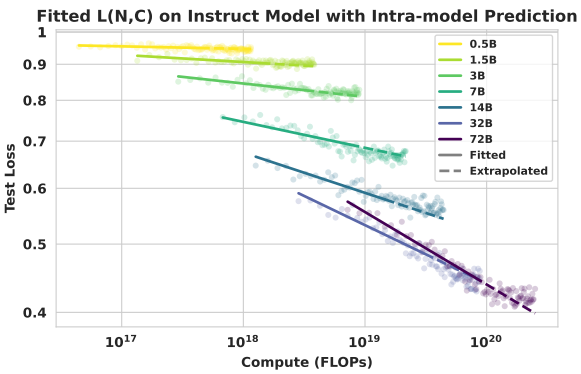

(d) Intra-model Prediction for Instruct Model

Figure 1: **Empirical Scaling Behaviors in RL Post-training.** We validate the proposed power-law (Eq. 1), which characterizes the relationship between model performance and post-training resource consumption, across models ranging from 0.5B to 72B parameters. **(a, b) Inter-model Prediction:** Scaling coefficients fitted on smaller models (0.5B–32B) accurately predict the learning efficiency of the held-out 72B model (dashed lines) . **(c, d) Intra-model Prediction:** The final convergence on the full dataset is extrapolated solely from early training dynamics.

scaling behavior can be effectively modeled by a power-law that exhibits a log-linear relationship between test loss and resource budget:

$$\log L(N, X) = -k(N) \cdot \log X + E(N) \quad (1)$$

Here, $k(N)$ represents the learning efficiency, which our empirical results show does not grow indefinitely with increasing model scale. Instead, it follows a saturation trend modeled by:

$$k(N) = \frac{K_{\max}}{1 + \frac{N_0}{N}} \quad (2)$$

This formulation (Eq. 2) shows that: while larger models consistently exhibit higher learning efficiency, the marginal gains in efficiency diminish as model size increases, asymptotically approaching a theoretical limit $K_{\max}$.

To empirically validate this law and determine its parameters, we fine-tune 63 LLMs with reinforcement learning on over 50k mathematics problems, based on the Qwen2.5 model family (Qwen et al., 2025). Figure 1 shows that, within the 0.5B-72B range, the loss reduction brought by RL follows an approximately log-linear trend with compute. Importantly, larger models not only have better initial performance but also generally have more efficiency in computation and data utilization during the optimization process. Further analysis confirms that our proposed formulation (Eq. 1) exhibits notable predictability, while also verifying the saturation effect in efficiency gains.

We additionally analyze the data-constrained regime, where we demonstrate that data reuse is a highly effective strategy. We validate the generality of our findings through extensive ablation studies on both base and instruct model series. Besides, we have also conducted experiments to study the impact of the rollout number in the GRPO algorithm (Shao et al., 2024), shown in Appendix B.2. These investigations establish fundamental scaling relationships for RL post-training, providing a

quantitative foundation and practical guidelines for resource-efficient model refinement.

Specifically, our key findings can be summarized as follows:

- **We propose a predictive power-law formulation for RL post-training**, which models the scaling relationship between test loss, model size, compute, and data. This formulation enables reliable prediction of both larger model performance and late-stage training trajectories.
- Larger models consistently exhibit superior compute and data efficiency in the RL post-training, but **the marginal gains in efficiency diminish gradually with increasing model scale**, revealing an inherent saturation trend.
- In data-limited settings, repeated exposure to a small dataset is nearly as effective as using larger corpora, **highlighting data reuse as a practical strategy**.

2 Experimental Setup

We describe the experimental setup for studying scaling behavior in RL post-training of LLMs for mathematical reasoning, including the model family, training and evaluation data, and evaluation protocol in this section. Full details are provided in Appendix A.

Models and Framework. We use the Qwen2.5 model family (0.5B, 1.5B, 3B, 7B, 14B, 32B and 72B parameters) (Qwen et al., 2025), which shares the same architecture, so that parameter count is the only variable in our scaling analysis. All experiments are run with the VeRL framework (Sheng et al., 2024), a large-scale RL platform for LLMs ensuring consistency and reproducibility.

Dataset settings. The training data is the mathematics subset of the `guru-RL-92k` dataset from the Reasoning360 project (Cheng et al., 2025), which is carefully curated through deduplication and difficulty filtering. We further sort the problems by increasing difficulty (decreasing pass rate, evaluated by Qwen2.5-7B-Instruct model) to enable curriculum learning. The evaluation data consists of two parts. To verify proposed scaling law (Eq. 1), we use a held-out set of 500 in-domain math problems sampled from the training distribution. To assess generalization, we evaluate on a broader benchmark suite spanning mathematics (AIME2024 (Patel et al., 2024), AMC2023 (KnovelEng, 2025), GSM8K (Cobbe et al., 2021), MATH500 (Lightman et al., 2023)), code (HumanEval (Chen et al., 2021)), logic (Zebra Puzzle(Lin, 2024)), and science (SuperGPQA (Team et al., 2025)). More details about dataset settings can be found in Appendix A.1.

Prompt Setting. To ensure stable behavior during RL training and evaluation, we use structured prompts tailored to each domain. For example, all mathematics problems are prepended with the Chain-of-Thought prompt (Wei et al., 2023): *"You are a knowledgeable math assistant. Answer the following questions and think step by step"*. More prompt templates for all related domains could be found in Appendix A.3.

RL Algorithm. We use Group Relative Policy Optimization (GRPO) (Shao et al., 2024) for RL fine-tuning. GRPO estimates advantages by normalizing rewards across responses sampled from the same prompt, yielding a stable signal with lower memory cost. Specifically, for each question q, GRPO samples a group of outputs$\{o_1, o_2, \cdots, o_G\}$ from the old policy $\pi_{\theta_{old}}$, and the objective is defined as

$$\mathcal{L}_{\text{GRPO}} = \frac{1}{G}\sum_{i=1}^{G}\frac{1}{|o_i|}\sum_{t=1}^{|o_i|}\Big\{\min\Big[\rho(\theta)\,\hat{A}_{i,t},\ \text{clip}\Big(\rho(\theta), 1-\varepsilon, 1+\varepsilon\Big)\hat{A}_{i,t}\Big] - \beta\,\mathrm{D}_{\text{KL}}\Big\}, \tag{3}$$

where $\rho(\theta) = \frac{\pi_\theta(o_{i,t}|q,o_{i,<t})}{\pi_{\theta_{\text{old}}}(o_{i,t}|q,o_{i,<t})}$ is the important sampling weight. For each output o_i, a reward model or rule is used to yield the reward signal $\mathbf{r} = \{r_1, r_2, \cdots, r_G\}$. The advantage is computed as

$$\hat{A}_{i,t} = \frac{r_i - \text{mean}(\mathbf{r})}{\text{std}(\mathbf{r})}. \tag{4}$$

Reward Signal and Evaluation Metric. For training, we use a binary reward signal in mathematical RL process, a reward of 1 is given for a correct match and 0 otherwise. For evaluation, we define our primary metric as the test loss (L), a proxy for reward-based performance in the RL setting. Formally, $L = 1 - (R/R_{\text{max}})$, where R is the number of correct solutions and R_{max} the total. We adopt the term "test loss" for consistency with foundational neural scaling law literature ((Kaplan et al., 2020)). Notably, maximizing reward in RL training is equivalent to minimizing L.

Fitting and Prediction Protocols. To systematically evaluate the robustness and predictive capability of our derived scaling laws, we employ two distinct fitting protocols throughout our analysis:

- **Inter-model Extrapolation:** We fit the scaling law parameters using data from smaller models (0.5B to 32B) to calculate the learning efficiency and predict the performance of the larger model (72B).
- **Intra-model Extrapolation:** We fit the scaling law using only the early training steps of a specific model to forecast its loss trajectory for the remainder of the training process.

3 Empirical Results and Scaling Laws

This section presents a comprehensive empirical investigation into the scaling behavior of RL for post-training LLMs. We first examine scaling behaviors under compute and data constraints, then analyze independent scaling dimensions, data reuse strategies, and finally evaluate generalization performance together. To ensure robust conclusions, each configuration is repeated **three times** for both base and instruct models ranging from 0.5B to 72B.Their **statistical uncertainty analysis**, including Average Standard Deviation and Standard Error of the Mean (SEM), are provided in Appendix C.3.

3.1 Compute-Optimal Scaling

To characterize the scaling behavior under computational limits, we first formalize the Compute-Constrained Scenario. Given a fixed computational budget C, we seek to identify the optimal model size N (and the corresponding data allocation D) that minimizes the final test loss. This can be expressed as the following constrained optimization problem:

$$\arg\min_{N,\,D} L(N, D) \quad \text{s.t.} \quad \text{FLOPs}(N, D) = C_{\text{const}}, \tag{5}$$

To solve this, we train 0.5B–72B models and measure test loss as a function of cumulative FLOPs C. As shown in Figure 1, larger models consistently outperform smaller ones under the same compute budget for both base and instruct variants. These plots include both Inter-model Extrapolation (fitted on 0.5B-32B and extrapolated on 72B) and Intra-model Prediction (predicting the remainder of training from initial steps) to demonstrate the predictive power of our derived scaling law. The loss–compute relationship follows a log-linear trend, which can be modeled by a power-law:

$$\log(L(N, C)) = -k_C(N) \cdot \log(C) + E_C(N),$$
$$\text{where } k_C(N) = \left(\frac{K_{Cmax}}{1 + \frac{N_C}{N}}\right) \tag{6}$$

To validate the predictive capability of Eq. 6, we conducted two levels of evaluation under the protocols defined in Section 2. First, applying **Inter-model Extrapolation**, we fitted the scaling parameters on smaller models (0.5B–32B) to estimate the learning efficiency $k_C(N)$ for the 72B model. As illustrated in Figure 1a and 1b, the predicted efficiency aligns closely with the actual performance of the 72B model. Second, using **Intra-model Prediction**, we forecasted the remaining loss trajectory of specific models based solely on early training steps (Figure 1c and 1d), confirming the formula's robustness across different training stages.

We further analyze learning efficiency term $k_C(N)$ in Eq. 6. As Figure 4a shows, $k_C(N)$ grows with model size N, meaning larger models consistently have higher learning efficiency. However, the efficiency gain from model scale is not uniformly linear. Beyond 32B, the increase in $k_C(N)$ diminishes, leading to efficiency saturation.

This saturation is manifested as a distinct performance crossover in Figure 1: In contrast to the immediate dominance of larger models in smaller parameter regimes, the 32B model outperforms the 72B counterpart initially under equivalent compute budgets, as the smaller model size inherently enables more training steps. We believe this observation reveals a latent trade-off between model scale and training steps in compute-constrained scenarios.

3.2 Data-Optimal Scaling

In many practical applications, the bottleneck lies not in compute but in the availability of high-quality reasoning data. We define the Data-Constrained Scenario as determining the model size N that yields the lowest test loss given a limited amount of unique training data D:

$$\arg\min_{N,\,C} L(N, C) \quad \text{s.t.} \quad D = D_{\text{const}}. \tag{7}$$

To empirically investigate this regime, we train models with varying parameter counts N on fixed

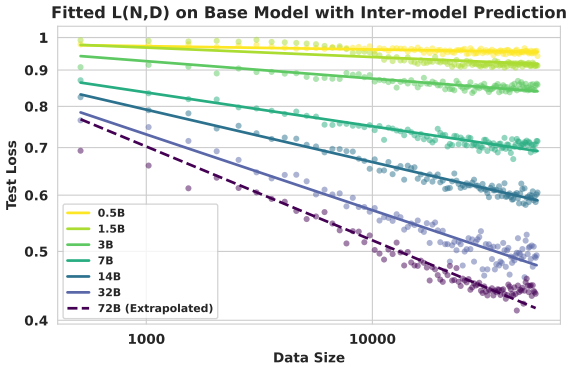

(a) Inter-model Prediction for Base Model

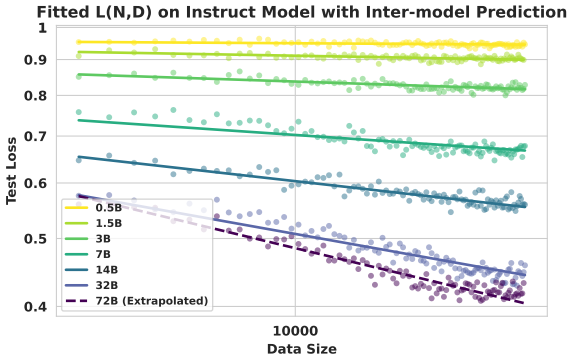

(b) Inter-model Prediction for Instruct Model

Figure 2: **Inter-model Prediction in data scenario.** The scaling law parameters are fitted on smaller models (0.5B–32B) to **predict** the learning efficiency of the largest model (72B, represented by dashed lines). The accurate alignment validates that the superior sample efficiency of larger models follows a predictable trajectory, confirming that performance gains scale consistently up to 72B.

amounts of unique samples D. As shown in Figure 2 and Figure 3, larger models consistently demonstrate superior sample efficiency within the 0.5B–72B range, achieving lower test loss under the same data constraints. This loss–data relationship also follows a log-linear trend and can be modeled by a formula analogous to the compute scenario:

$$\log(L(N,D)) = -k_D(N)\cdot\log(D) + E_D(N),$$
$$\text{where } k_D(N) = \left(\frac{K_{Dmax}}{1+\frac{N_D}{N}}\right) \tag{8}$$

Mirroring the analysis in Section 3.1, we evaluate the predictive capability of our data scaling law (Eq. 8) in two consistent settings: inter-model extrapolation (Shown in Figures 2) and intra-model prediction (Shown in Figures 3), and the predictions also align with actual results closely. We further find that, with the same analytic form, the data learning efficiency $k_D(N)$ follows a saturation curve identical to $k_C(N)$: as illustrated in Figure 4b, larger models outperform smaller ones in extracting knowledge from each data point, yet efficiency gains diminish at scales beyond 32B. The unified functional form across both compute and data domains underscores the theoretical consistency of our scaling law.

3.3 Scaling with Constrained Data and Reuse

When unique data is scarce, a critical question is whether repeating data is effective. We investigate this Data Reuse Scenario by fixing the total data budget and varying the reuse factor τ. Specifically,

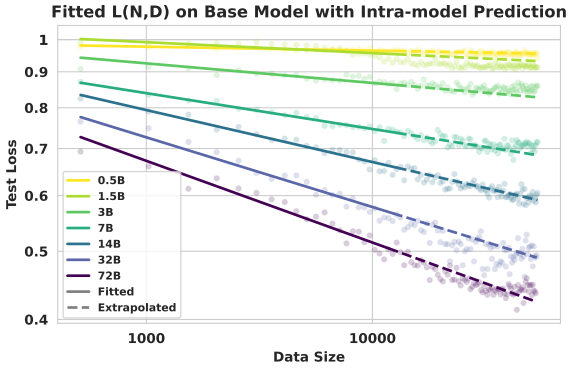

(a) Intra-model Prediction for Base Model

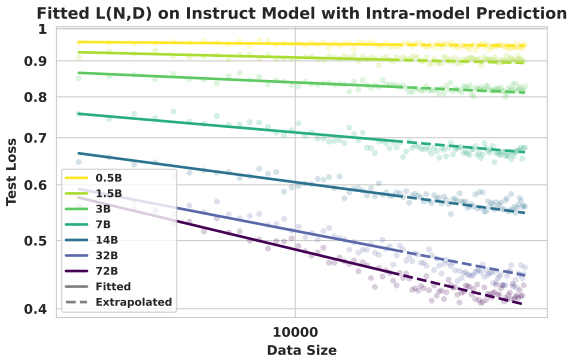

(b) Intra-model Prediction for Instruct Model

Figure 3: **Intra-model Prediction in data scenario.** The loss trajectory is fitted using initial training data steps to **predict** the subsequent performance trends on the full dataset. The results demonstrate that RL post-training maintains a nearly constant learning efficiency (manifesting as a linear trend in log-scale) during the rapid performance ascent, allowing the overall training trajectory to be accurately extrapolated from early dynamics.

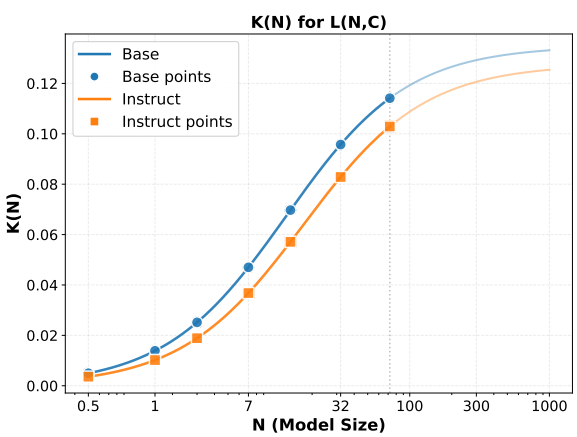

(a) Fitted learning efficiency $k_C(N)$.

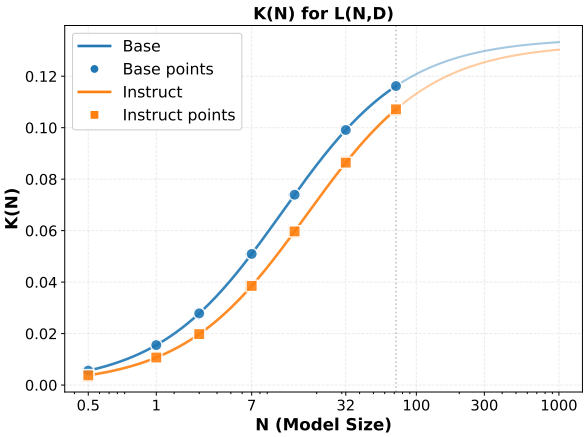

(b) Fitted learning efficiency $k_D(N)$.

Figure 4: Fitted learning efficiency coefficients for Base and Instruct models. Both $k_C(N)$ (a) and $k_D(N)$ (b) exhibit identical trends: larger models consistently show higher learning efficiency, with efficiency gains beginning to diminish after the 32B model size.

we aim to identify the optimal reuse factor τ that minimizes the test loss:

$$\underset{\tau}{\text{argmin}}; L(\tau) \quad \text{s.t.} \quad D_{\text{unique}} \times \tau = D_{\text{total}}, \quad (9)$$

To systematically evaluate this problem, we simulate data constraints by partitioning the training set into smaller subsets while preserving the difficulty distribution (Details provided in Appendix A.4). Each subset is cycled through multiple times, with τ controlling the repetition frequency. Crucially, the total number of used data D_{total} is kept fixed across runs, and curriculum ordering is maintained to ensure that performance differences arise solely from the degree of data reuse rather than distributional artifacts.

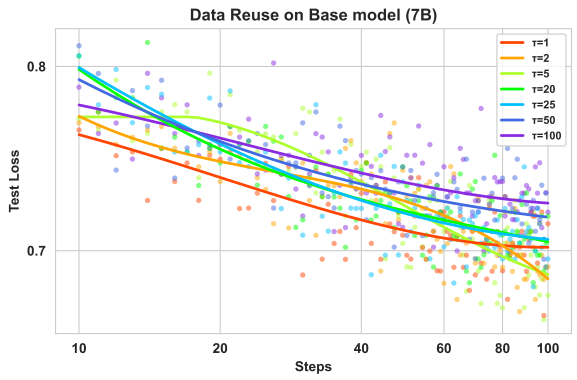

Figure 5: Performance in data-constrained settings is primarily determined by the total number of used data (D_{total}). For a fixed D_{total}, the final test loss is insensitive to the data reuse factor (τ), with no significant degradation up to $\tau = 25$.

Under this experimental setup, our results demonstrate that performance is primarily governed by the total number of optimization steps (D_{total}), rather than sample uniqueness. As illustrated in Figure 5 (for instruct model, check Figure 8 in Appendix A.4), the final test loss proves insensitive to the reuse factor, showing no significant degradation for $\tau \leq 25$. However, the limit exists at $\tau = 100$, we observe clear signs of overfitting, indicating that excessive repetition eventually harms generalization. Collectively, these findings confirm that moderate data reuse is a highly effective strategy for RL fine-tuning in data-constrained regimes.

3.4 Domain Transfer

We investigate the generalization capabilities of reinforcement learning fine-tuning (RFT) by evaluating models on a comprehensive suite of in-domain and out-of-domain (OOD) benchmarks. Our results demonstrate a divergent trends: while RL post-training yields robust generalization improvements on in-domain mathematical tasks of varying difficulty, it shows negligible transfer to out-of-domain tasks. (Detailed results are provided in Appendix B.1).

In-Domain Generalization. Figure 6 shows consistent improvements on unseen mathematics tasks outside the training set. On benchmarks, from easy to hard, including `GSM8K`, `MATH-500`, `AMC2023`, `AIME2024`, test loss steadily decreases with training compute, suggesting that RL post-training enhances transferable reasoning skills within mathematics.

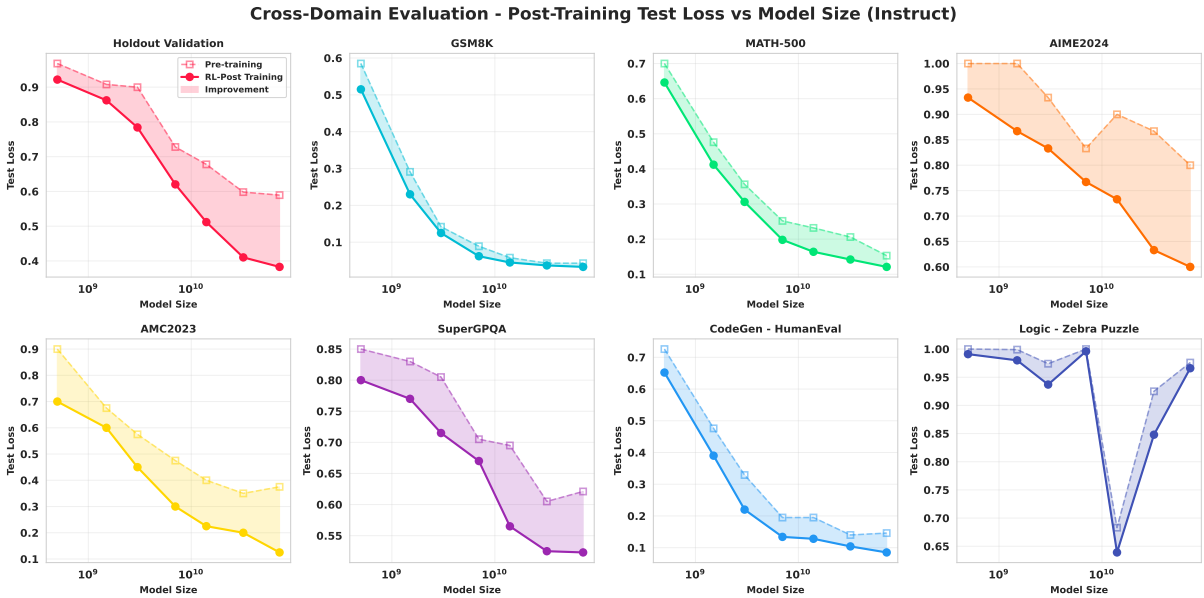

Figure 6: RL post-training on mathematical reasoning yields generalization improvements on in-domain tasks with varying difficulty, but shows negligible transfer to out-of-domain tasks.

Out-of-Domain Generalization. As shown in Figure 6, results on OOD tasks are markedly different. For code generation (`HumanEval`) and STEM problems (`SuperGPQA`), performance gains marginally, indicating that RL fine-tuning is highly specialized.On logical reasoning (`zebra_puzzle`), performance degrades for larger models, suggesting that intensive optimization on mathematical reasoning may interfere with or "damage" other distinct reasoning abilities.

4 Related Work

Foundational Scaling Laws of Neural Language Models. Foundational scaling studies show language modeling loss follows smooth power-laws in model size N, data D, and compute C (Kaplan et al., 2020), with compute-optimal training prescribing near lockstep growth of parameters and tokens under fixed FLOPs (Hoffmann et al., 2022). Later analyses attribute earlier discrepancies to embedding/non-embedding parameter accounting, last-layer costs, optimizer warmup, and scale-sensitive hyperparameters (Pearce and Song, 2024; Porian et al., 2024), while data-centric refinements examine pruning efficiency (Sorscher et al., 2022), repetition effects (Hernandez et al., 2022), gzip-based complexity predictors (Pandey, 2024), constrained or synthetic regimes (Muennighoff et al., 2023; Qin et al., 2025), and task transfer (e.g., translation) (Isik et al., 2024). Test-time compute amplification supplies an inference analogue to classical training laws (Snell et al., 2024).

RL post-training in LLMs. In RL, power-law trends similarly link capacity, interaction compute, and performance (Hilton et al., 2023); scaling RFT across horizon and compute improves mathematical and coding reasoning (DeepSeek-AI, 2025; Kimi Team, 2025; Mai et al., 2025b; Zhang et al., 2025a,b), while extended schedules (Liu et al., 2025), ultra-low-shot or single-example RL (Wang et al., 2025), and minimal-data efficiency paradigms (Li et al., 2025b) probe data–compute tradeoffs. Instability and uneven gains highlight fragile optimization (Zeng et al., 2025a; Yue et al., 2025), and multi-domain mixtures reveal both synergy and interference across math, code, and logic (Li et al., 2025c; Cheng et al., 2025).

Mathematical Reasoning with LLMs. Mathematical reasoning amplifies these dynamics: accuracy generally scales upward while verification behaviors remain inconsistent (Touvron et al., 2023); corpus volume and quality jointly shape attainable curves (Ye et al., 2024); multi-task math-generalist training diverges from specialist scaling trajectories (Yue et al., 2023); and RL with code execution induces additional behaviors such as emergent tool use concentrated in math problem solving (Zeng et al., 2025b). Collectively, evidence indicates that reasoning performance is governed by interacting axes of model size, data distribution/quality, training (supervised vs. RL) paradigm, and allocation

of both training and inference compute, while unified laws for mathematical reasoning remain only partially characterized.

5 Discussion

Scaling Dependence on Evaluation Environment and Metrics. Reinforcement learning optimizes directly for environment rewards (Sutton and Barto, 2018), which in principle allows unbounded capability—as demonstrated by AlphaZero mastering board games (Silver et al., 2017), AlphaFold predicting protein structures (Jumper et al., 2021), and frontier LLMs such as Gemini-2.5-Pro achieving IMO-level performance (Huang and Yang, 2025). In contrast, text-based LLMs lack a well-defined RL environment, forcing us to rely on human-curated datasets as proxies. Test loss thus serves as a pragmatic but imperfect metric: it is monotonic and convergent, yet heavily dependent on dataset construction and task difficulty, with different benchmarks (e.g., GSM8K vs. AIME, Section 3.4) showing distinct convergence rates. This task dependence makes the absolute coefficients of our fitted scaling laws (K_{max}, N_0, E) difficult to interpret universally. Prior work proposed "intrinsic performance"—the minimum compute needed to reach a target reward—as a normalization across environments (Hilton et al., 2023), but we did not find an analogous measure in large-scale LLMs. Establishing principled, environment-independent evaluation protocols remains an open and critical challenge for RL-based scaling studies.

Scaling Dependence on Model Scale. Our study of models from 0.5B to 72B parameters shows that larger models exhibit greater sample and compute efficiency in RL post-training. This parameter range allows us to characterize the scaling limits. We found that these advantages do not extend indefinitely. Our analytic learning efficiency term $k(N)$ in Eq.6 and Eq.8, explicitly confirms that the efficiency gains follow a saturation curve toward a limit ($K_{\max}$). This finding implies that scaling up models beyond a certain point, while still yielding absolute performance gains, suffers from diminishing marginal returns in efficiency.

Dependence on RL Algorithm. Our analysis is based on GRPO, a mainstream and stable RL post-training algorithm for LLMs that uses an actor-only design and normalizes rewards across responses. Comparative study with alternative RL algorithms (Cui et al., 2025) reports minor differences in training curves. Whether more advanced algorithms can significantly improve sample efficiency or stability—and thereby reshape the scaling frontier—remains an important open question.

Future of LLM Agent. The integration of reinforcement learning with agentic LLMs is increasingly viewed as a promising direction (Zhang et al., 2025a,b). Both theoretical and empirical studies show that augmentations such as external tool use and long-term memory can substantially boost model performance (Lin and Xu, 2025; Houliston et al., 2025; Mai et al., 2025a). We anticipate that such agentic mechanisms will markedly improve the scaling behavior of RL-trained LLMs: by offloading deterministic computations to tools and focusing learning on high-level decision making, these models could achieve much higher efficiency, effectively shifting the performance frontier upward for a given compute or data budget. Understanding the scaling laws of these agentic systems is, therefore, a key and exciting avenue for future research.

6 Conclusion

In this work, we conducted a comprehensive empirical study to characterize the scaling behaviors of reinforcement learning post-training for large language models. Our analysis yields three fundamental findings:

First, we establish a predictive power-law formulation that models the log-linear relationship between test loss and resource consumption. We demonstrate that this formulation enables reliable performance forecasting, accurately predicting the learning efficiency of larger model and estimating final trajectories from early training dynamics.

Second, we identify a inherent saturation trend in learning efficiency. While larger models consistently exhibit superior compute and sample efficiency, the marginal gains in the learning efficiency coefficient $k(N)$ do not grow indefinitely; instead, they diminish as model size increases, asymptotically approaching a theoretical limit.

Third, we find that RL model performance in data-constrained regimes is primarily governed by the total volume of training data rather than sample uniqueness. Our experiments validate that moderate data reuse is a highly effective strategy, where increasing the repetition factor allows models to maintain performance improvements without requiring additional unique samples.

Limitations

First, our conclusions are currently limited to reinforcement learning within the mathematical domain and have not yet been extended to multi-domain RL scenarios. Second, constrained by the Qwen2.5 series limit of 72B parameters, we could not empirically verify the efficiency saturation trend on larger-scale models beyond this size. Finally, our experiments focus exclusively on the Qwen dense model family; the generalizability of these findings to other architectures, such as Llama or Mixture-of-Experts (MoE) models, remains to be explored.

References

Janice Ahn, Rishu Verma, Renze Lou, Di Liu, Rui Zhang, and Wenpeng Yin. 2024. Large language models for mathematical reasoning: Progresses and challenges. In *Proceedings of the 18th Conference of the European Chapter of the Association for Computational Linguistics: Student Research Workshop*, pages 225–237, St. Julian's, Malta. Association for Computational Linguistics.

Mark Chen, Jerry Tworek, Heewoo Jun, Qiming Yuan, Henrique Ponde de Oliveira Pinto, Jared Kaplan, Harri Edwards, Yuri Burda, Nicholas Joseph, Greg Brockman, Alex Ray, Raul Puri, Gretchen Krueger, Michael Petrov, Heidy Khlaaf, Girish Sastry, Pamela Mishkin, Brooke Chan, Scott Gray, and 39 others. 2021. Evaluating large language models trained on code. *Preprint*, arXiv:2107.03374.

Zhoujun Cheng, Shibo Hao, Tianyang Liu, Fan Zhou, Yutao Xie, Feng Yao, Yuexin Bian, Yonghao Zhuang, Nilabjo Dey, Yuheng Zha, Yi Gu, Kun Zhou, Yuqi Wang, Yuan Li, Richard Fan, Jianshu She, Chengqian Gao, Abulhair Saparov, Haonan Li, and 5 others. 2025. Revisiting reinforcement learning for llm reasoning from a cross-domain perspective. *arXiv preprint arXiv:2506.14965*.

Karl Cobbe, Vineet Kosaraju, Mohammad Bavarian, Mark Chen, Heewoo Jun, Lukasz Kaiser, Matthias Plappert, Jerry Tworek, Jacob Hilton, Reiichiro Nakano, Christopher Hesse, and John Schulman. 2021. Training verifiers to solve math word problems. *Preprint*, arXiv:2110.14168.

Ganqu Cui, Yuchen Zhang, Jiacheng Chen, Lifan Yuan, Zhi Wang, Yuxin Zuo, Haozhan Li, Yuchen Fan, Huayu Chen, Weize Chen, Zhiyuan Liu, Hao Peng, Lei Bai, Wanli Ouyang, Yu Cheng, Bowen Zhou, and Ning Ding. 2025. The entropy mechanism of reinforcement learning for reasoning language models. *Preprint*, arXiv:2505.22617.

DeepSeek-AI. 2025. Deepseek-r1: Incentivizing reasoning capability in llms via reinforcement learning. *arXiv preprint arXiv:2501.12948*.

Mohamed Amine Ferrag, Norbert Tihanyi, and Merouane Debbah. 2025. From llm reasoning to autonomous ai agents: A comprehensive review. *arXiv preprint arXiv:2504.19678*.

Danny Hernandez, Tom Brown, Tom Conerly, Nova DasSarma, Dawn Drain, Sheer El-Showk, Nelson Elhage, Zac Hatfield-Dodds, Tom Henighan, Tristan Hume, and 1 others. 2022. Scaling laws and interpretability of learning from repeated data. *arXiv preprint arXiv:2205.10487*.

Jacob Hilton, Jie Tang, and John Schulman. 2023. Scaling laws for single-agent reinforcement learning. *arXiv preprint arXiv:2301.13442*.

Jordan Hoffmann, Sebastian Borgeaud, Arthur Mensch, Elena Buchatskaya, Trevor Cai, Eliza Rutherford, Diego de Las Casas, Lisa Anne Hendricks, Johannes Welbl, Aidan Clark, Tom Hennigan, Eric Noland, Katie Millican, George van den Driessche, Bogdan Damoc, Aurelia Guy, Simon Osindero, Karen Simonyan, Erich Elsen, and 3 others. 2022. Training compute-optimal large language models. In *Proceedings of the 36th International Conference on Neural Information Processing Systems*, NIPS '22, Red Hook, NY, USA. Curran Associates Inc.

Sam Houliston, Ambroise Odonnat, Charles Arnal, and Vivien Cabannes. 2025. Provable benefits of in-tool learning for large language models. *Preprint*, arXiv:2508.20755.

Yichen Huang and Lin F. Yang. 2025. Gemini 2.5 pro capable of winning gold at imo 2025. *Preprint*, arXiv:2507.15855.

Berivan Isik, Natalia Ponomareva, Hussein Hazimeh, Dimitris Paparas, Sergei Vassilvitskii, and Sanmi Koyejo. 2024. Scaling laws for downstream task performance in machine translation. *arXiv preprint arXiv:2402.04177*.

John Jumper, Richard Evans, Alexander Pritzel, Tim Green, Michael Figurnov, Olaf Ronneberger, Kathryn Tunyasuvunakool, Russ Bates, Augustin Žídek, Anna Potapenko, and 1 others. 2021. Highly accurate protein structure prediction with alphafold. *nature*, 596(7873):583–589.

Jared Kaplan, Sam McCandlish, Tom Henighan, Tom B Brown, Benjamin Chess, Rewon Child, Scott Gray, Alec Radford, Jeffrey Wu, and Dario Amodei. 2020. Scaling laws for neural language models. *arXiv preprint arXiv:2001.08361*.

Kimi Team. 2025. Kimi k1.5: Scaling reinforcement learning with llms. *arXiv preprint arXiv:2501.12599*.

KnovelEng. 2025. Knovel engineering amc-23 dataset. https://huggingface.co/datasets/knoveleng/AMC-23. Accessed: 2025-09-23.

Margaret Li, Sneha Kudugunta, and Luke Zettlemoyer. 2025a. (mis)fitting scaling laws: A survey of scaling

law fitting techniques in deep learning. In *The Thirteenth International Conference on Learning Representations*.

Xuefeng Li, Haoyang Zou, and Pengfei Liu. 2025b. Limr: Less is more for rl scaling. *arXiv preprint arXiv:2502.11886*.

Yu Li, Zhuoshi Pan, Honglin Lin, Mengyuan Sun, Conghui He, and Lijun Wu. 2025c. Can one domain help others? a data-centric study on multi-domain reasoning via reinforcement learning. *arXiv preprint arXiv:2507.17512*.

Hunter Lightman, Vineet Kosaraju, Yura Burda, Harri Edwards, Bowen Baker, Teddy Lee, Jan Leike, John Schulman, Ilya Sutskever, and Karl Cobbe. 2023. Let's verify step by step. *Preprint*, arXiv:2305.20050.

Bill Yuchen Lin. 2024. ZeroEval: A Unified Framework for Evaluating Language Models.

Heng Lin and Zhongwen Xu. 2025. Understanding tool-integrated reasoning. *Preprint*, arXiv:2508.19201.

Mingjie Liu, Shizhe Diao, Ximing Lu, Jian Hu, Xin Dong, Yejin Choi, Jan Kautz, and Yi Dong. 2025. Prorl: Prolonged reinforcement learning expands reasoning boundaries in large language models. *arXiv preprint arXiv:2505.24864*.

Xinji Mai, Haotian Xu, Zhong-Zhi Li, Xing W, Weinong Wang, Jian Hu, Yingying Zhang, and Wenqiang Zhang. 2025a. Agent rl scaling law: Agent rl with spontaneous code execution for mathematical problem solving. *Preprint*, arXiv:2505.07773.

Xinji Mai, Haotian Xu, Weinong Wang, Jian Hu, Yingying Zhang, Wenqiang Zhang, and 1 others. 2025b. Agent rl scaling law: Agent rl with spontaneous code execution for mathematical problem solving. *arXiv preprint arXiv:2505.07773*.

Niklas Muennighoff, Alexander Rush, Boaz Barak, Teven Le Scao, Nouamane Tazi, Aleksandra Piktus, Sampo Pyysalo, Thomas Wolf, and Colin A Raffel. 2023. Scaling data-constrained language models. *Advances in Neural Information Processing Systems*, 36:50358–50376.

OpenAI, :, Sandhini Agarwal, Lama Ahmad, Jason Ai, Sam Altman, Andy Applebaum, Edwin Arbus, Rahul K. Arora, Yu Bai, Bowen Baker, Haiming Bao, Boaz Barak, Ally Bennett, Tyler Bertao, Nivedita Brett, Eugene Brevdo, Greg Brockman, Sebastien Bubeck, and 108 others. 2025. gpt-oss-120b and gpt-oss-20b model card. *Preprint*, arXiv:2508.10925.

Rohan Pandey. 2024. gzip predicts data-dependent scaling laws. *arXiv preprint arXiv:2405.16684*.

Bhrij Patel, Souradip Chakraborty, Wesley A. Suttle, Mengdi Wang, Amrit Singh Bedi, and Dinesh Manocha. 2024. Aime: Ai system optimization via multiple llm evaluators. *Preprint*, arXiv:2410.03131.

Tim Pearce and Jinyeop Song. 2024. Reconciling kaplan and chinchilla scaling laws. *arXiv preprint arXiv:2406.12907*.

Tomer Porian, Mitchell Wortsman, Jenia Jitsev, Ludwig Schmidt, and Yair Carmon. 2024. Resolving discrepancies in compute-optimal scaling of language models. *Advances in Neural Information Processing Systems*, 37:100535–100570.

Zeyu Qin, Qingxiu Dong, Xingxing Zhang, Li Dong, Xiaolong Huang, Ziyi Yang, Mahmoud Khademi, Dongdong Zhang, Hany Hassan Awadalla, Yi R Fung, and 1 others. 2025. Scaling laws of synthetic data for language models. *arXiv preprint arXiv:2503.19551*.

Qwen, :, An Yang, Baosong Yang, Beichen Zhang, Binyuan Hui, Bo Zheng, Bowen Yu, Chengyuan Li, Dayiheng Liu, Fei Huang, Haoran Wei, Huan Lin, Jian Yang, Jianhong Tu, Jianwei Zhang, Jianxin Yang, Jiaxi Yang, Jingren Zhou, and 25 others. 2025. Qwen2.5 technical report.

Zhihong Shao, Peiyi Wang, Qihao Zhu, Runxin Xu, Junxiao Song, Xiao Bi, Haowei Zhang, Mingchuan Zhang, Y. K. Li, Y. Wu, and Daya Guo. 2024. Deepseekmath: Pushing the limits of mathematical reasoning in open language models. *Preprint*, arXiv:2402.03300.

Guangming Sheng, Chi Zhang, Zilingfeng Ye, Xibin Wu, Wang Zhang, Ru Zhang, Yanghua Peng, Haibin Lin, and Chuan Wu. 2024. Hybridflow: A flexible and efficient rlhf framework. *arXiv preprint arXiv: 2409.19256*.

David Silver, Thomas Hubert, Julian Schrittwieser, Ioannis Antonoglou, Matthew Lai, Arthur Guez, Marc Lanctot, Laurent Sifre, Dharshan Kumaran, Thore Graepel, Timothy Lillicrap, Karen Simonyan, and Demis Hassabis. 2017. Mastering chess and shogi by self-play with a general reinforcement learning algorithm. *Preprint*, arXiv:1712.01815.

Charlie Snell, Jaehoon Lee, Kelvin Xu, and Aviral Kumar. 2024. Scaling llm test-time compute optimally can be more effective than scaling model parameters. *arXiv preprint arXiv:2408.03314*.

Ben Sorscher, Robert Geirhos, Shashank Shekhar, Surya Ganguli, and Ari Morcos. 2022. Beyond neural scaling laws: beating power law scaling via data pruning. *Advances in Neural Information Processing Systems*, 35:19523–19536.

Richard S. Sutton and Andrew G. Barto. 2018. *Reinforcement Learning: An Introduction*. A Bradford Book, Cambridge, MA, USA.

P Team, Xinrun Du, Yifan Yao, Kaijing Ma, Bingli Wang, Tianyu Zheng, King Zhu, Minghao Liu, Yiming Liang, Xiaolong Jin, Zhenlin Wei, Chujie Zheng, Kaixin Deng, Shawn Gavin, Shian Jia, Sichao Jiang, Yiyan Liao, Rui Li, Qinrui Li, and 78 others. 2025. Supergpqa: Scaling llm evaluation across 285 graduate disciplines. *Preprint*, arXiv:2502.14739.

Hugo Touvron, Albert Q. Jiang, Nan Du, and et al. 2023. Scaling relationship on learning mathematical reasoning with large language models. *arXiv preprint arXiv:2308.01825*.

Yiping Wang, Qing Yang, Zhiyuan Zeng, Liliang Ren, Liyuan Liu, Baolin Peng, Hao Cheng, Xuehai He, Kuan Wang, Jianfeng Gao, and 1 others. 2025. Reinforcement learning for reasoning in large language models with one training example. *arXiv preprint arXiv:2504.20571*.

Jason Wei, Xuezhi Wang, Dale Schuurmans, Maarten Bosma, Brian Ichter, Fei Xia, Ed Chi, Quoc Le, and Denny Zhou. 2023. Chain-of-thought prompting elicits reasoning in large language models. *Preprint*, arXiv:2201.11903.

An Yang, Anfeng Li, Baosong Yang, Beichen Zhang, Binyuan Hui, Bo Zheng, Bowen Yu, Chang Gao, Chengen Huang, Chenxu Lv, Chujie Zheng, Dayiheng Liu, Fan Zhou, Fei Huang, Feng Hu, Hao Ge, Haoran Wei, Huan Lin, Jialong Tang, and 41 others. 2025. Qwen3 technical report. *Preprint*, arXiv:2505.09388.

Qiwei Ye, Chenxin Qian, Qingxiu Song, and et al. 2024. Skywork-math: Data scaling laws for mathematical reasoning in large language models — the story goes on. *arXiv preprint arXiv:2407.08348*.

Xiang Yue, Fanghua Liu, Yuxuan Zhang, and et al. 2023. Mammoth: Building math generalist models. *arXiv preprint arXiv:2309.05653*.

Yang Yue, Zhiqi Chen, Rui Lu, Andrew Zhao, Zhaokai Wang, Shiji Song, and Gao Huang. 2025. Does reinforcement learning really incentivize reasoning capacity in llms beyond the base model? *arXiv preprint arXiv:2504.13837*.

Weihao Zeng, Yuzhen Huang, Qian Liu, Wei Liu, Keqing He, Zejun Ma, and Junxian He. 2025a. Simplerl-zoo: Investigating and taming zero reinforcement learning for open base models in the wild. *arXiv preprint arXiv:2503.18892*.

Yifan Zeng, Tianyu Guo, Yuqing Wang, and et al. 2025b. Agent rl scaling law: Spontaneous code execution for mathematical problem solving. *arXiv preprint arXiv:2505.07773*.

Guibin Zhang, Hejia Geng, Xiaohang Yu, Zhenfei Yin, Zaibin Zhang, Zelin Tan, Heng Zhou, Zhongzhi Li, Xiangyuan Xue, Yijiang Li, Yifan Zhou, Yang Chen, Chen Zhang, Yutao Fan, Zihu Wang, Songtao Huang, Yue Liao, Hongru Wang, Mengyue Yang, and 6 others. 2025a. The landscape of agentic reinforcement learning for llms: A survey. *Preprint*, arXiv:2509.02547.

Kaiyan Zhang, Yuxin Zuo, Bingxiang He, Youbang Sun, Runze Liu, Che Jiang, Yuchen Fan, Kai Tian, Guoli Jia, Pengfei Li, Yu Fu, Xingtai Lv, Yuchen Zhang, Sihang Zeng, Shang Qu, Haozhan Li, Shijie Wang, Yuru Wang, Xinwei Long, and 20 others. 2025b. A survey of reinforcement learning for large reasoning models. *Preprint*, arXiv:2509.08827.

A Experiment Setup Details

This section provides a detailed breakdown of the datasets and hyperparameters used in our experiments. All experiments were conducted on a cluster of NVIDIA H200 GPUs.

A.1 Dataset Details

Our training was conducted on a curated mathematics dataset. For evaluation, especially for analyzing generalization (as mentioned in the main text), we utilized a comprehensive suite of benchmarks spanning multiple domains. The composition of this evaluation suite is detailed in Table 1.

A.2 Hyperparameter Configuration

All experiments were conducted with a consistent set of hyperparameters for the Group Relative Policy Optimization (GRPO) algorithm to ensure a fair comparison across different model sizes and configurations. The key hyperparameters are listed in Table 2.

Hyperparameter	Value
Learning Rate	$1e-6$
Batch Size	512
KL Loss Coefficient	0.001
Rollout Temperature (Training)	1.0
Rollout Temperature (Evaluation)	0.7
Clip Ratio (High & Low)	0.2
Input Sequence Length	2048
Output Sequence Length	4096

Table 2: GRPO training hyperparameters used across all experiments.

A.3 Prompt Templates

This section details the specific prompt templates used for evaluating models on different domains. For each task, the model was provided with the corresponding instruction prepended to the problem statement `<question>`. Check the details in Table 3.

A.4 Data Reuse Experiment Setup

To systematically evaluate the effect of data reuse under constrained data scenarios, we design controlled experiments where all runs are trained with the same total data size but different levels of data

Dataset	Samples	Huggingface Tag	Domain
Held-out Data	500	LLM360/guru-RL-92k	Math
aime2024	30	Maxwell-Jia/AIME_2024	Math
amc2023	40	knoveleng/AMC-23	Math
codegen_humaneval	164	openai/openai_humaneval	Code
gsm8k	1319	openai/gsm8k	Math
logic_zebra_puzzle	200	LLM360/guru-RL-92k	Logical Reasoning
math	500	HuggingFaceH4/MATH-500	Math
stem_supergpqa	200	LLM360/guru-RL-92k	STEM
Total	**2953**		

Table 1: Composition of the multi-domain evaluation suite.

Domain	Prompt Template
Mathematics	`You are a knowledgeable math assistant. Answer the following questions and think step by step\n<question>\nPlease output the final answer within \\boxed{}.`
Code	`Write a complete, self-contained Python solution to the following problem. Your solution must include all necessary imports and the full function definition, including the signature exactly as specified. Do not modify the function signature or docstring.\n<question>`
Logic	`Solve the following puzzle\n<question>\nPlease return the final answer in <answer> </answer> tags, for example <answer> {"header": ["Position", "Nationality", "Job"], "rows": [["1", "british", "plumber"], ["2", "polish", "carpenter"]]} </answer>.`
Science (STEM)	`You are a knowledgeable assistant. Answer the following questions and think step by step \n <question> \n put your final answer option within \\boxed{}. Only put the letter in the box, e.g. \\boxed{A}. There is only one correct answer`

Table 3: Prompt templates used for different evaluation domains.

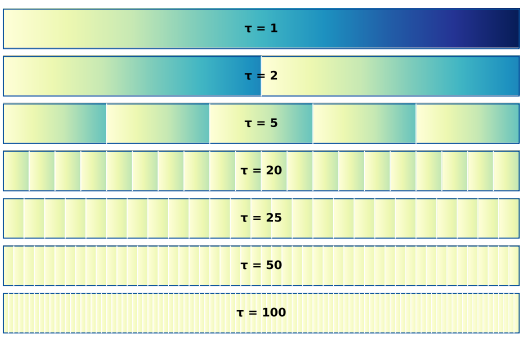

Figure 7: Data Reuse Schema

H

repetition. Each run randomly samples a subset from the full training corpus and repeats this subset sufficiently many times to exactly match the target data budget (i.e., subset size $\times\ \tau\ =$ total data size). Unlike (Muennighoff et al., 2023), subsets are sampled independently for each run rather than sampling within the larger subsets, to mitigate sampling bias and balance stochasticity across conditions. To remain consistent with the Curriculum Learning setting of the main experiments, examples within each subset are ordered by increasing difficulty; across epochs, this difficulty schedule is preserved and repeated rather than reshuffled, as illustrated in Figure 7. We also put the results for instruct model in Figure 8.

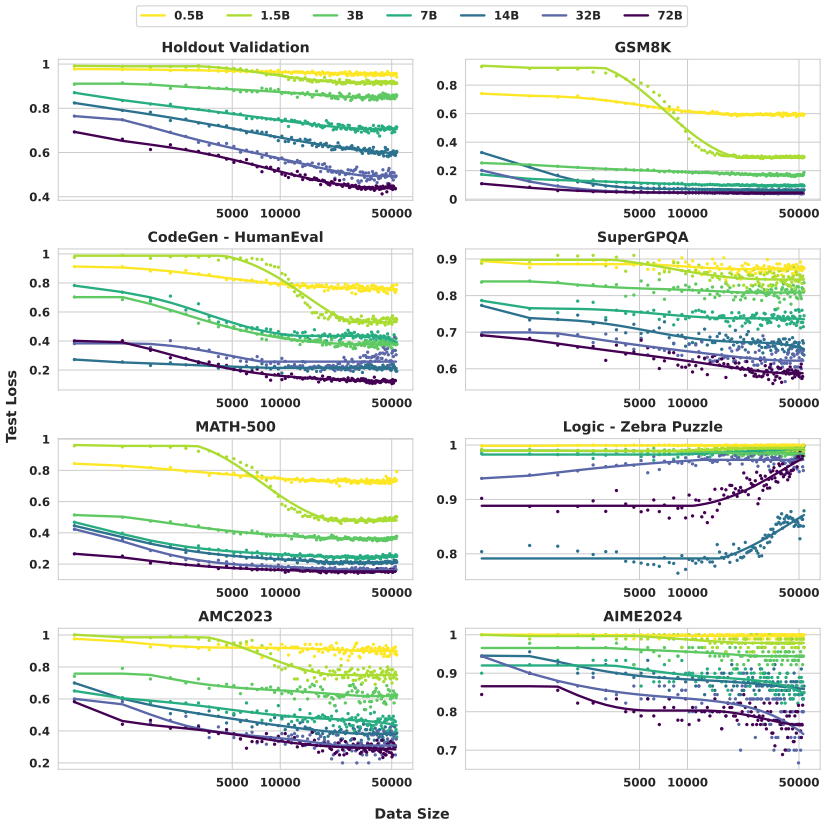

Figure 9: Test loss on in-domain and out-of-domain benchmarks vs data size for Base models. It shows modest positive transfer on in-domain tasks, with limited or negative transfer on OOD tasks.

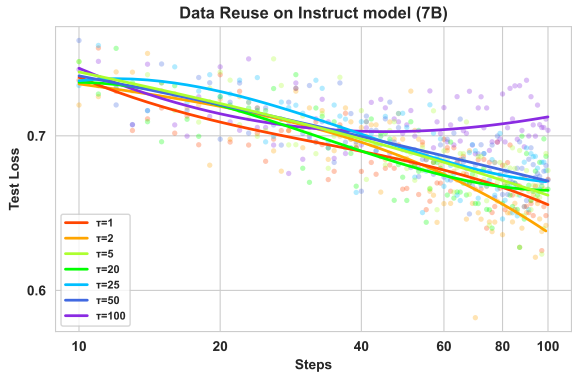

Figure 8: Instruct Model

B Additional Experiment Results

This section provides supplementary experimental results that support and extend the analyses presented in the main body of the paper.

B.1 Performance on In-Domain and Out-of-Domain Tasks

To assess how the mathematical reasoning capabilities acquired during RL fine-tuning generalize, we evaluated our models on a comprehensive suite of unseen benchmarks. We categorize these into two groups: in-domain different tasks (other mathematics datasets) and out-of-domain tasks (e.g., code, science, logic). The results are presented in Figure 9 and Figure 10.

In-Domain Generalization (Different Mathematical Tasks). On mathematics benchmarks not included in our training set (such as GSM8K, MATH, AIME, and AMC), we observe a generally positive transfer of learned skills. For most of these tasks, the test loss shows a modest but consistent decrease as training progresses, particularly for the larger models. This suggests that the model's enhanced reasoning ability is not overfitted to the training distribution and is applicable to a wider range of mathematical problems.

Out-of-Domain Generalization. When evaluating on tasks outside of mathematics, the generalization is more limited. For both code generation (HumanEval) and science problems (SuperGPQA), performance remains largely static throughout the training process across all model sizes, with test loss curves staying flat. This indicates that the specialized mathematical reasoning skills do not readily transfer to these domains. A noteworthy phe-

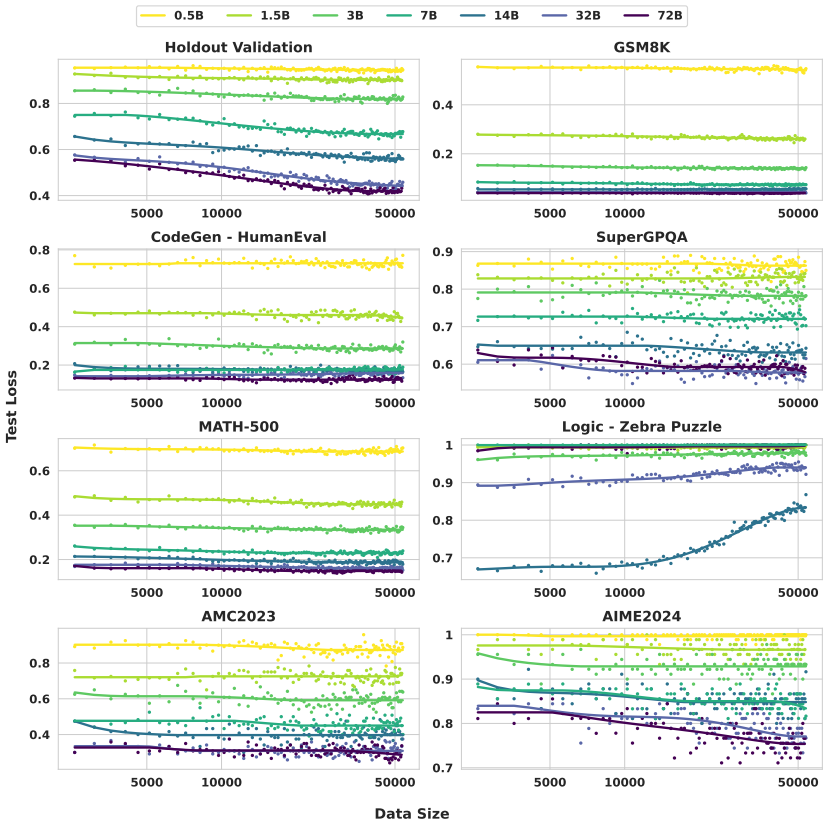

Figure 10: Test loss on in-domain and out-of-domain benchmarks vs data size for Instruct models.

nomenon is observed in the logical reasoning task (Zebra Puzzle): the largest models (particularly the 14B variants) show a degradation in performance (an increase in test loss) as training progresses, suggesting a potential negative transfer effect where intensive optimization on mathematical reasoning may interfere with capabilities required for certain types of logical puzzles.

B.2 Ablation on GRPO Hyperparameters

We conducted an ablation study on the rollout group size G, a key GRPO hyperparameter that controls how many responses are sampled per prompt. This directly affects both the compute per update and the stability of the training signal. We tested $G \in \{4, 8, 16, 32\}$ on the 7B models.

Data-centric View. Figure 11b and 11d shows that larger rollout sizes consistently yield better sample efficiency: $G = 32$ achieves the lowest test loss for the same number of unique samples. This supports the intuition that more responses per question provide a stronger advantage estimate and thus more effective gradient updates.

Compute-centric View. The optimal rollout size G is not fixed but shifts with the training budget. This implies that practitioners should tune G according to available compute rather than relying on a universal setting. We attribute this dynamic to the trade-off between the higher variance reduction from larger G and the additional FLOPs it consumes, which makes small G preferable at low budgets but large G superior when ample compute is available.

B.3 Peformance Compared with Advance Models

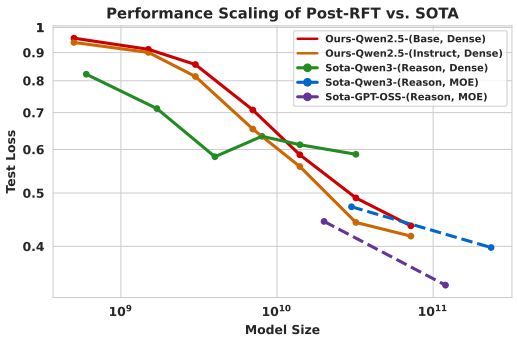

Figure 12: Relation between test loss and model size N for our trained model and SOTA models demonstrates the effectiveness of our training.

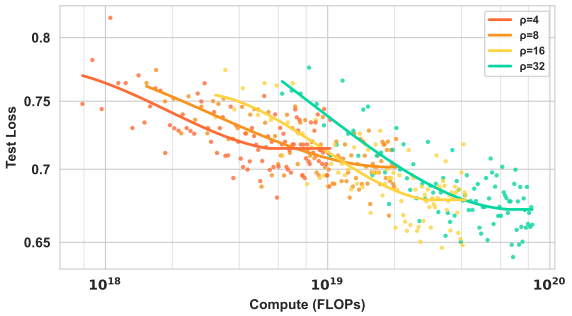

(a) 7B-Base: Loss vs. Compute

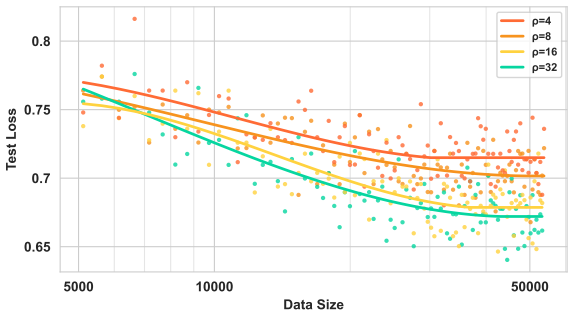

(b) 7B-Base: Loss vs. Data Size

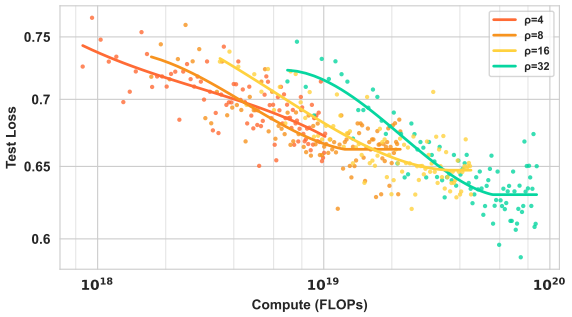

(c) 7B-Instruct: Loss vs. Compute

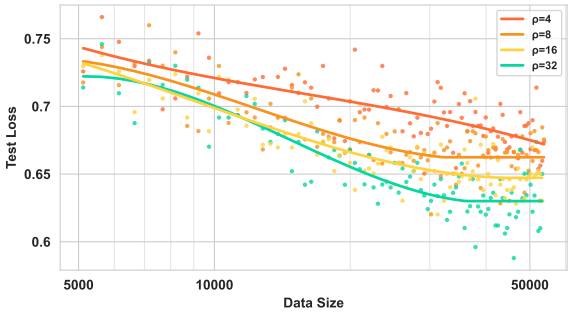

(d) 7B-Instruct: Loss vs. Data Size

Figure 11: Effects of GRPO rollout size on training efficiency. The top row shows the base model results, while the bottom row shows the instruct model results.

We train models of varying sizes to convergence and compare their final test loss. As shown in Figure 12, larger models consistently achieve lower loss, improving monotonically with scale. The curve shows that smaller models get weaker gains, suggesting diminishing returns at low parameter counts. A likely reason is that larger models inherit richer pre-trained representations, which reinforcement fine-tuning exploits for greater improvements than parameter growth alone.

We also benchmark our RL-tuned Qwen2.5 models (Qwen et al., 2025) against state-of-the-art open-source reasoning systems, including Qwen3 (Yang et al., 2025) and GPT-OSS (OpenAI et al., 2025), detailed in Table 4. On our held-out set, the 32B and 72B models match or surpass dense Qwen3 counterparts of similar size, highlighting the effectiveness of RL post-training. Mixture-of-experts models such as Qwen3 and GPT-OSS achieve approximate loss at much larger scales (235B), with GPT-OSS-120B currently leading. These comparisons suggest that scaling across 0.5B-72B will be necessary to fully characterize post-training behavior and compete with frontier MoE systems.

Model Family	Model Identifier	Pass@1 Score
Models from Our Study (Post-RFT)		
Qwen2.5-Base	0.5B	0.070
	1.5B	0.116
	3B	0.182
	7B	0.338
	14B	0.450
	32B	0.540
	72B	0.607
Qwen2.5-Instruct	0.5B	0.078
	1.5B	0.138
	3B	0.216
	7B	0.380
	14B	0.488
	32B	0.590
	72B	0.617
External SOTA Models (for Comparison)		
Qwen3	0.6B	0.178
	1.7B	0.288
	4B	0.418
	8B	0.366
	14B	0.388
	30B (A3B)	0.528
	32B	0.412
	235B (A22B)	**0.602**
GPT-OSS	20B	0.556
	120B	**0.660**

Table 4: Performance of various models on the held-out evaluation set.

To contextualize the performance of our models and the difficulty of our primary evaluation metric, we benchmarked a range of external, state-of-the-art (SOTA) models on our held-out mathematics test set. The results are presented in Table 4. The performance of our Qwen2.5 models reflects their final scores after the completion of reinforcement learning fine-tuning (RFT), while others are benchmarked directly.

C Formula Fitting and Derivation

C.1 FLOPs Calculation Methodology

The computational cost for a LLM is primarily determined by the number of non-embedding parameters (N) and the number of processed tokens (T). The costs for the fundamental operations are:

- **Forward Pass Cost:** The cost of a single forward pass is approximately $C_{\text{fwd}} \approx 2NT$ FLOPs.
- **Backward Pass Cost:** The backward pass is approximately twice as expensive as the forward pass, so $C_{\text{bwd}} \approx 4NT$ FLOPs.

A full training step, which includes one forward and one backward pass for the gradient update, therefore has a total computational cost of:

$$C_{\text{train}} = C_{\text{fwd}} + C_{\text{bwd}} \approx 2NT + 4NT = 6NT \text{ FLOPs}. \quad (10)$$

$$\text{FLOPs}_{\text{step}} = 6 \times N \times T_{\text{step}} \quad (11)$$

By recording the exact number of processed tokens T per step, we compute the cumulative FLOPs reported throughout this paper as the sum of these per-step calculations over the course of training.

C.2 Coefficient Comparison

We consider the two laws

$$\ln L(N, C) = -k_C(N)\,\ln C + E_C(N), \quad (12)$$

and

$$\ln L(N, D) = -k_D(N)\,\ln D + E_D(N), \quad (13)$$

are consistent under the linkage $C = ND\phi$ where $\phi > 0$ is a constant for simplification.

Claim. Under $C = ND\phi$, the slopes coincide and the intercepts differ by a known shift:

$$k_C(N) = k_D(N) \;=\; k(N), \quad (14)$$

$$E_C(N) = E_D(N) \;+\; k(N)\,\ln\big(N\phi\big). \quad (15)$$

Proof. Substitute $C = ND\phi$ into equation 12:

$$\begin{aligned}\ln L(N, C) &= -k_C(N)\ln(ND\phi) + E_C(N) \\ &= -k_C(N)\big[\ln D + \ln(N\phi)\big] + E_C(N) \\ &= -k_C(N)\ln D \\ &\quad + \Big(E_C(N) - k_C(N)\ln(N\phi)\Big).\end{aligned}$$

Comparing this with equation 13, i.e., $\ln L(N, D) = -k_D(N)\,\ln D + E_D(N)$, equality for all $D > 0$ forces the coefficients of $\ln D$ and the constants to match:

$$k_D(N) = k_C(N) =: k(N),$$
$$E_D(N) = E_C(N) - k(N)\,\ln(N\phi).$$

Rearranging the second identity yields equation 15.

The observation from Figure 4a and Figure 4b also matches with this conclusion.

C.3 Hyper-parameter Fitting

We present the uncertainty analysis for raw data and fitting results for hyper parameters in Table 5 and Table 6.

D A Loss Decomposition Model for Scaling Analysis

During the analysis, we found a more generalized form of the potential scaling law function that fits the curves well. This model fits the same dataset as the main experiments and is included here as a formally documented alternative for future research.

D.1 Loss Decomposition Model

The General Loss Decomposition. We construct the generalized formula as follows, based on the observation of the loss composition of post-training and the experiment data:

$$L(N, D) = L_\infty + G(N) + \lambda(N) \cdot P(N, D) \quad (16)$$

Each term in Equation equation 16 represents a clear part decomposing the loss:

- L_∞ denotes the **irreducible loss**, representing the fundamental loss floor that persists even with infinite model capacity and unlimited data. It reflects task-intrinsic uncertainty and noise that cannot be eliminated by improved modeling or additional training, such as inherent stochasticity in the environment or irreducible mismatch between training and evaluation distributions.

Model	Base			Instruct		
	Test Loss	Avg Std	SEM	Test Loss	Avg Std	SEM
0.5B	0.9419	0.0082	0.0048	0.9458	0.0073	0.0042
1B	0.9129	0.0091	0.0053	0.8988	0.0098	0.0057
3B	0.8582	0.0129	0.0074	0.8281	0.0112	0.0065
7B	0.7148	0.0147	0.0085	0.6777	0.0142	0.0082
14B	0.6051	0.0149	0.0086	0.5588	0.0143	0.0083
32B	0.4937	0.0056	0.0032	0.4579	0.0127	0.0073
72B	0.4359	0.0143	0.0082	0.4320	0.0140	0.0081

Table 5: Uncertainty Analysis for raw data: Base and Instruct Models (Holdout Score)

Source	Metric	Scenario	k_{max}	N_0 (B)	R^2
Base	L(N,C)	Intra-model	0.1349	13.09	0.9955
	L(N,C)	Inter-model	0.1518	17.37	0.9944
	L(N,D)	Intra-model	0.1348	11.52	0.9953
	L(N,D)	Inter-model	0.1631	16.95	0.9947
Instruct	L(N,C)	Intra-model	0.1276	17.27	0.9970
	L(N,C)	Inter-model	0.1443	28.33	0.9950
	L(N,D)	Intra-model	0.1325	17.08	0.9970
	L(N,D)	Inter-model	0.1484	27.15	0.9949

Table 6: Comparison of k_{max} and N_0 Parameters Across Fitting Scenarios

- $G(N)$ denotes the **model-limited loss**, capturing the asymptotic loss floor imposed by finite model capacity N in the limit of infinite data. It corresponds to the capacity-dependent performance frontier of models with size N.
- $\lambda(N)$ denotes the **learnable capacity**, defined as the maximum achievable reduction in loss that a model of size N can attain through post-training, beyond its model-limited loss. In RL post-training settings, this term can depend on the pretraining regime, as well as the degree of mismatch between the pretraining and post-training task settings. Conceptually, the learnable capacity is governed by two opposing effects: larger models generally have greater capacity to extract and acquire new knowledge, while simultaneously having already absorbed more information during pretraining, leaving less headroom for additional improvement via RL. As a result, the monotonic dependence of $\lambda(N)$ on model size is non-trivial, and its precise modeling likely requires additional assumptions and empirical characterization.
- $P(N, D)$ denotes the **learning progress**, a normalized function taking values in $[0, 1]$ that quantifies the fraction of the learnable capacity $\lambda(N)$ realized when training on a dataset of size D.

Instantiated Model. Following prior empirical scaling law studies, we parameterize the model-limited loss as

$$G(N) = \left(\frac{N_0}{N}\right)^{\alpha}, \tag{17}$$

reflecting the observed power-law dependence of loss on model size in the infinite-data regime (Kaplan et al., 2020).

Empirically, learning curves exhibit an S-shaped transition when plotted in log–log coordinates (e.g. Figure 1). Motivated by this observation, we model the learning progress term $P(N, D)$ as a logistic function in $\log D$,

$$P(N, D) = \frac{1}{1 + \left(\frac{D}{D_0(N)}\right)^{\beta}}, \tag{18}$$

where $D_0(N)$ denotes the characteristic dataset scale at which half of the learnable capacity is realized, and is treated as a N-dependent parameter.

Combining the above components, we arrive at the following instantiated loss model:

$$L(N, D) = L_\infty + \left(\frac{N_0}{N}\right)^{\alpha} + \frac{\lambda(N)}{1 + \left(\frac{D}{D_0(N)}\right)^{\beta}} \tag{19}$$

This is what we used to fit and extrapolation in Figure 13

D.2 Predictability and Extrapolation

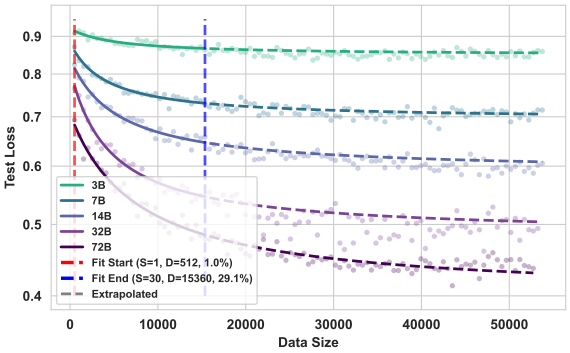

(a) Intra-model prediction using the early 30% of training steps.

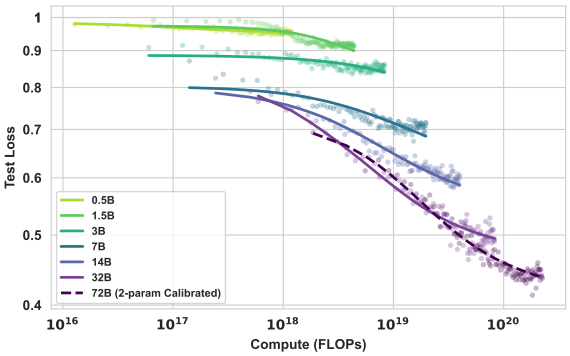

(b) Inter-model extrapolation for 72B under fixed shared shape.

Figure 13: Extrapolation of the loss decomposition model (Equation equation 19). (a) Intra-model prediction using partial learning-curve observations. (b) Inter-model extrapolation for 72B with global exponents fixed from smaller models.

We evaluate the extrapolation behavior of the loss–decomposition model (Equation equation 19) by applying it to the same experimental learning-curve data used in the main analysis, and by testing its performance under two complementary settings (Figure 13).

Intra-model prediction. Using only the first 30% of training steps for each model, the fitted curves closely match the held-out portions(Figure 13a). This indicates that the internal S-shaped structure of the model provides a sufficiently strong inductive bias for completing a single learning curve from early observations. See Table 7 for detailed fitting result.

Inter-model extrapolation. We fit all global exponents and the model-limited term using models up to 32B, and then extrapolate the resulting shared functional form to 72B by calibrating only two model-specific parameters, $\lambda(72\text{B})$ and $D_0(72\text{B})$. The extrapolated curve aligns well with the observed 72B trajectory across the full data range, reflecting that the functional shape inferred from smaller models remains compatible with larger-scale behavior under this light calibration.

The fit is reasonably strong, indicating that the proposed formulation may capture key structural tendencies of the underlying scaling behavior.

Table 7: Fitting details for $L(N, D)$ using only 30% of the training steps for each model.

Model Size	Base		
	D_0	$lambda$	R^2
3B	5109.6316	0.0734	0.995
7B	3725.6374	0.1882	0.995
14B	4554.7619	0.2520	0.995
32B	3576.0323	0.3279	0.995
72B	5861.6228	0.3084	0.995

D.3 Discussion: Effective log–log slope

To relate the loss decomposition model to the slope-based formulation used in the main text, we examine the local behavior of $L(N, D)$ in log–log coordinates with respect to the data scale D. Specifically, we define the effective slope

$$k(N, D) := -\frac{\partial \log L(N, D)}{\partial \log D},$$

which corresponds to the exponent in a local power-law approximation of the form $\log L \approx -k \log D +$ const.

For the loss decomposition model (Equation equation 19), the induced $k(N, D)$ is a smooth function of D that vanishes in both the low-data and high-data limits, and attains its maximum around the characteristic scale $D \approx D_0(N)$. Evaluating the slope at this point yields a natural definition of the maximal effective slope,

$$k_{\max}(N) = \frac{K_{\max}}{1 + S(N)}, \tag{20}$$

$$K_{\max} := \frac{\beta}{2}, \tag{21}$$

$$S(N) := \frac{2(L_\infty + (N_0/N)^\alpha)}{\lambda(N)}. \tag{22}$$

The resulting $k_{\max}(N)$ depends only on the model size N through the parameters of the loss decomposition, and is uniformly bounded by $K_{\max} = \beta/2$.

From this perspective, the slope function $k(N)$ adopted in the main analysis (Equation equation 2) can be interpreted as a parsimonious, low-parameter approximation to the effective maximal slope $k_{\max}(N)$ in Eq. 20. This establishes structural consistency between the two descriptions: the loss decomposition model potentially captures the finer-grained (N, D)-dependent behavior, while the main-text formulation summarizes its dominant N-dependent trend in a compact form.

D.4 Conclusion

The loss decomposition model captures key empirical characteristics of RL post-training scaling behavior.

However, several components remain underdetermined, including the construction of the learnable capacity $\lambda(N)$, the dependence of the characteristic dataset scale $D_0(N)$ on model size, the role of the pretraining process, and the impact of mismatches between pretraining and post-training task settings.

For these reasons, we present this model as an appendix-level discussion rather than a core component of the main text. We encourage future work to build on this formulation to further investigate and refine scaling laws for LLM-based reinforcement learning.

E Response Length

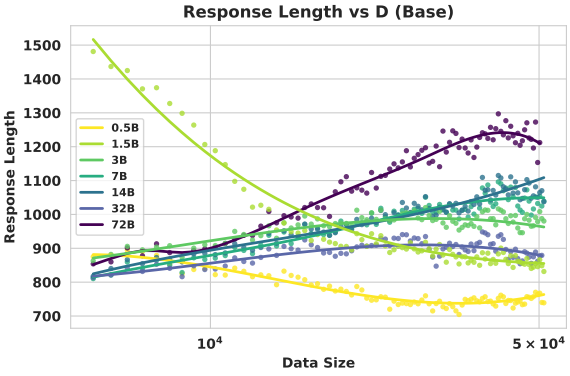

Figure 14: Response length vs. Data size (Base models).

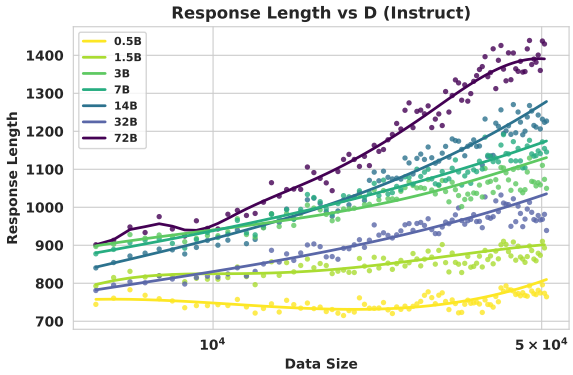

Figure 15: Response length vs. Data size (Instruct models).

F Ethics Statement

This work is foundational in nature, focusing on the scaling properties of large language models in the domain of mathematical reasoning. Our research exclusively utilizes publicly available and previously published resources, including open-source models (e.g., Qwen2.5) and established datasets (e.g.,guru-RL-92k), thereby mitigating concerns related to data privacy, human subjects, or the release of sensitive information. The application domain of mathematical problem-solving does not inherently present risks of direct societal harm. The primary ethical consideration associated with this work is the environmental impact of the computational resources required for large-scale model training, a challenge common to the field. We believe that by providing insights into efficient resource allocation, our work contributes positively to mitigating this concern for future research.

G The Use of Large Language Models

We used Large Language Model (LLM) to refine our initial draft. This process included checking for obvious grammatical and syntactical errors, as well as making the language more formal and academic. We reviewed the content generated by the LLM to ensure that no prohibited generated content appeared in the article.